Int J Adv Manuf Technol (2015) 80:959–969
DOI 10.1007/s00170-014-6613-x

ORIGINAL ARTICLE

Experimental and numerical study on hydroforming characteristics of friction stir welded aluminum alloy tubes

Z. L. Hu · X. S. Wang · Q. Pang · F. Huang · X. P. Qin · S. J. Yuan · L. Hua

Received: 27 April 2014 / Accepted: 18 November 2014 / Published online: 11 April 2015

Abstract Friction stir welding (FSW), as a solid state joining technique, has emerged as an efficient method for manufacturing tailor-welded blanks to optimize weight or performance in the final component. As the basic design of lightweight frame structures in the automotive and aircraft industry is frequently based on tubular profiles, the joining strategies and forming technologies have to be developed accordingly. In the present study, FSW tube was produced by a novel processing sequence. The plastic deformation characteristics during hydroforming were experimentally and numerically investigated with two types of end condition. The hydroforming performance of the FSW tubes was mainly investigated by die-bulge forming with fixed ends, and the wrinkling behavior during hydroforming was analyzed by employing axial feed on the tube ends. It is found that hydroforming FSW tube is a new deal and does show a few peculiarities. The FSW tube exhibits a spiral weld and the basin-shaped nugget. Fine-grained structure is retained during tube forming. The thinning of the tube in axial direction shows M-shaped distribution during hydroforming. The severe thinning is observed at one quarter of the expansion zone from symmetry plane. In the hoop direction, the base material near the weld suffers severe thinning due to the high hoop and axial tensile stress. The thickness distribution greatly depends on the sequence of the contacting die and the variations of the curvature radius of the tube during hydroforming. Moreover, the weld shows an inhibitory effect for the generation of the wrinkles and decreases the number of the wrinkles as compared to the seamless tube during hydroforming. This effect is more obvious when the forming pressure is lower.

Keywords Friction stir welding · Aluminum alloy · Hydroforming · Plastic deformation

Z. L. Hu (✉) · F. Huang · X. P. Qin · L. Hua
Hubei Key Laboratory of Advanced Technology of Automobile Parts, Wuhan University of Technology, Wuhan 430070, People's Republic of China
e-mail: zhilihuhit@163.com

Z. L. Hu · X. S. Wang · S. J. Yuan
State Key Laboratory of Advanced Welding and Joining, Harbin Institute of Technology, Harbin 150001, People's Republic of China

Q. Pang
School of Mechanical and Electrical Engineering, Wuhan Donghu University, Wuhan 430070, People's Republic of China

Z. L. Hu
State Key Laboratory of Materials Processing and Die & Mould Technology, Huazhong University of Science and Technology, Wuhan, People's Republic of China

1 Introduction

Lightweight construction is a central challenge in modern transportation engineering due to economical and ecological reason, to improve product properties. The application of lightweight construction can be realized by optimized structural design and usage of light materials, such as aluminum alloy and magnesium alloy. However, there are several barriers to the increased use of Al alloy in vehicle weight reduction applications such as room temperature formability, limitations within the existing manufacturing infrastructure, and poor weldability. Moreover, the lightweight design often increases the shape complexity of products and thus makes them difficult to be formed by conventional manufacturing technology.

Hydroforming, as one of the most effective ways to manufacture lightweight hollow structures with complicated cross sections, has been widely used in the automotive and aircraft industries for an effort to decrease vehicle weight and improve fuel economy. Dohmann and Hartl described the basic process as follows: a high-pressure internal fluid is combined with the

axial feeding simultaneously, forcing the tube to expand within a closed die to take the shape of the die cavity [1]. As compared with conventional manufacturing processes, this process showed greater advantages, such as better structural integrity, weight and cost reduction, increased strength, and reduction in part numbers [2, 3].

Friction stir welding (FSW), as a solid state joining technique, has emerged as an efficient manufacturing method for joining materials that can vary in composition and/or thickness to optimize weight or performance in the final component. Buffa et al. successfully adopted the FSW to produce an aluminum alloy tailored blanks. They pointed out that the welding parameters of FSW Al 7075-T6 tailored blanks had to be carefully designed in order to obtain high-quality joints [4]. Sato et al. examined the relationship between the microstructure of the FSW and its formability for the 5052 aluminum alloys. The results showed that the fracture limit strain of plane strain deformation increased with increasing subgrain size in the stir zone [5]. Miles et al. analyzed the formability of the AA 5754-O, AA 5182-O, and AA 6022-T4 aluminum alloy FSW joints by transverse tensile tests and the Limit Dome Height (LDH) and Ohio State University (OSU) tests. It was reported that the 5xxx series alloys had similar tensile ductility and formability to those of the unwelded base material near plane strain. However, the FSW 6022-T4 sheets only retained about 43 % of the base material tensile elongation and had rapidly decreasing formability as biaxial strain conditions were approached [6]. Although the FSW process was observed to offer better joint efficiency than fusion welding processes, the gap of the strength values and formability between the base metal and the weld metal was still large.

Limiting formability was also determined by experimentally investigating the possibility to form friction stir welded tubes. Fratini and Piacentini presented the application of FSW process to the joining of 6016-T4 aluminum alloy tube with a thickness of 3 mm, and the results showed that just 35 % of tensile strength of base material (BM) was obtained [7]. Dubourg et al. showed the preliminary results on friction stir welding of 2.7-mm-thick 2024-T3 aluminum alloy tubes with a circumferential weld. The tensile test results showed a 75 % drop in total elongation due to underfill defect presented on the weld [8]. Marré et al. investigated the feasibility of friction stir welding tubes by using a self-developed clamping device. It was reported that the macrosection was free of any joint defect, except for an excess weld metal of about 0.2 mm in the center because of the incomplete contact between the tool shoulder and the work pieces [9]. Urso et al. published some works on the weldability of aluminum tubes by means of FSW process, and the influence of the welding process on weld quality was investigated, namely feed rate and rotational speed [10, 11]. A preliminary analysis of the mechanical properties of friction stir welded tube by means of tube bulge test was also carried out. It was found that the process was robust only when specific clamping and welding devices were developed [11]. Leitao et al. concluded that important information was still required on the metallurgical and mechanical characterization of the welds when applying FSW in the production of tailor-welded blanks/tubes [12]. Until recently, research on the FSW had been limited mostly to its process mechanics, material flow, and metallurgical aspects in the experiments and numerical simulations [13, 14]. Studies on the macroscopic behavior of friction stir welded tailor-welded blank (TWB) sheets were rare except for a few recent works [15–17]. Silva et al. investigated the single-point incremental forming (SPIF) of tailored welded blanks produced by FSW, and the formability of the tailor-welded blanks was evaluated by means of benchmark tests [15]. Kim et al. experimentally and numerically investigated formability of the friction stir welded TWB sheets, and the main objective was to experimentally evaluate the formability performance by simple tension test, hemisphere dome stretching, and cylindrical cup drawing tests [16]. However, all these research studies were just performance evaluation. The mechanisms which affect formability of friction stir welded TWB sheets, especially the plastic deformation characteristics, were not investigated in detail. The published data was even scarcer when it came to the FSW tubes.

The authors had published some works on formability of the FSW blanks/tubes [18–20]. It was concluded that the main reasons for the decrease of the formability of the FSW blanks/tubes were the excess thickness reduction of the weld and the non-uniform deformation due to the heterogeneous microstructure distribution [18]. To solve the difficulty in the fabrication of FSW tubes and improve the formability, Hu et al. proposed a new method for producing FSW tube. The excess thickness reduction of the weld was avoided and the microstructure heterogeneity of FSW tube was also significantly improved [19]. A preliminary examination of the formability of the FSW tube by free bulge test was reported, and the tube exhibited high formability due to the homogeneous deformation of the weld and the BM [20]. However, the hydroforming characteristics of FSW tubes in the die-bulge forming, as well as the wrinkling behavior of the tube, were not elaborated in detail. It is known that the thinning of the tube is an important indicator to evaluate the quality of the hydroforming. It can fully reflect the characteristics of hydroforming. Therefore, we expand on these aspects more explicitly in the current paper. Hydroforming

according to its process features is classified by Dohmann and Hartl as follows: hydroforming tubes with a straight axis and hydroforming tubes with a bent centerline [1]. For the tubes with a bent centerline, the axial feeding always provides limited material flow due to friction and geometry constraint during hydroforming. While for the tubes with a straight axis, axial feed is expected to delay tube thinning and promote tube bulging. On the basis of the above considerations, the present study provides an examination of the hydroforming characteristics of the FSW tube with two types of end condition. The hydroforming performance of the FSW tubes is mainly investigated by die-bulge forming with fixed ends, and the wrinkling behavior during hydroforming is analyzed by employing axial feed on the tube ends.

2 Experimental procedure

Five-millimeter-thick 2024-O aluminum alloy rolled plates were coiled, and FSWwith a travel speed, a rotational speed, and a shoulder diameter of 100–300 mm/min, 600 rpm, and 14 mm, respectively, was conducted. After FSW, the tubes were spun at 200 °C to obtain the FSW tubes with an outer diameter of 103 mm and thickness of 1.5 mm. Since it was proved that the plasticity of the FSW joint was improved by post-weld heat treatment in our previous works, the heat treatment was conducted to the FSW tube followed by the tube forming operation. The heat treatment process was conducted at temperature of 300 °C for 2 h and then was cooled in the furnace to 200 °C.

The hydroforming characteristics of FSW tube were evaluated by hydroforming a tube with variable diameter. The tubes with variable cross section were very common parts in the automotive and aircraft industry, and hydroforming the tubes with variable cross section was one of the popular methods used to evaluate the hydroforming characteristics and plastic deformation law for circular tubes [21]. Figure 1 shows the shape and dimensions of the tube with variable diameter. The maximum diameter of the part was 124 mm and the expansion ratio was 20.3 %. Taking into account the classification of hydroforming, two types of end condition were employed on the tube ends and the wrinkling behavior during hydroforming was analyzed, as illustrated in Fig. 2. The machine employed in the process was a 1000-t hydroforming press, which was designed and fabricated at Harbin Institute of Technology and capable of applying pre-programmed routes of axial feed and internal pressure.

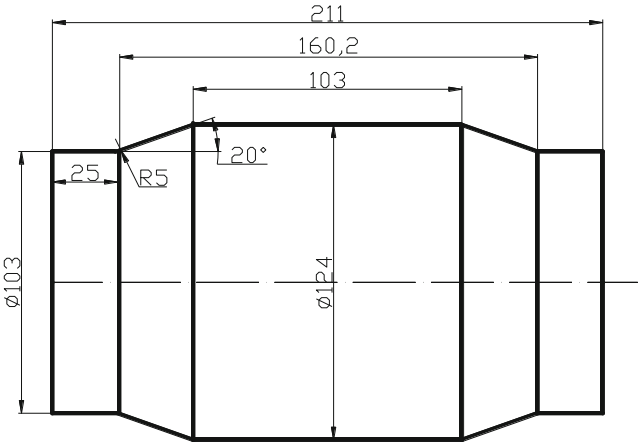

Fig. 1 Shape and dimensions of the part (mm)

3 Experimental results

3.1 Hydroforming FSW tube without axial feeding

Figure 3 shows the FSW tube obtained by the new process. The FSW tube shows good weld quality with a smooth upper surface, and no obvious wall thickness reduction and crack are observed. It is interesting that the initial straight weld is changed into a spiral weld (Fig. 3a). Moreover, a basin-shaped nugget that widens near the upper surface can be seen in the whole tube forming process (Fig. 3b, c), even after heat treatment at 300 °C (Fig. 3d). It is indicated that the weld is stable and the fine equiaxed grain structure is supposed to be retained during tube forming.

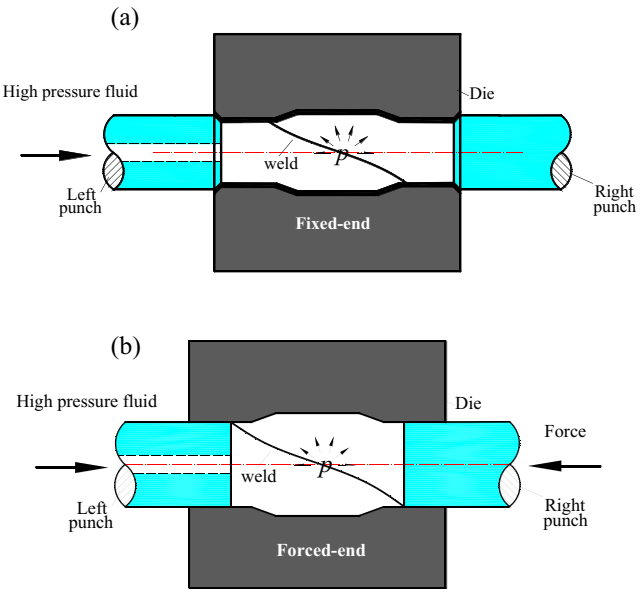

Fig. 2 Schematic illustration of the end conditions used during hydroforming: **a** fixed-end and **b** forced-end

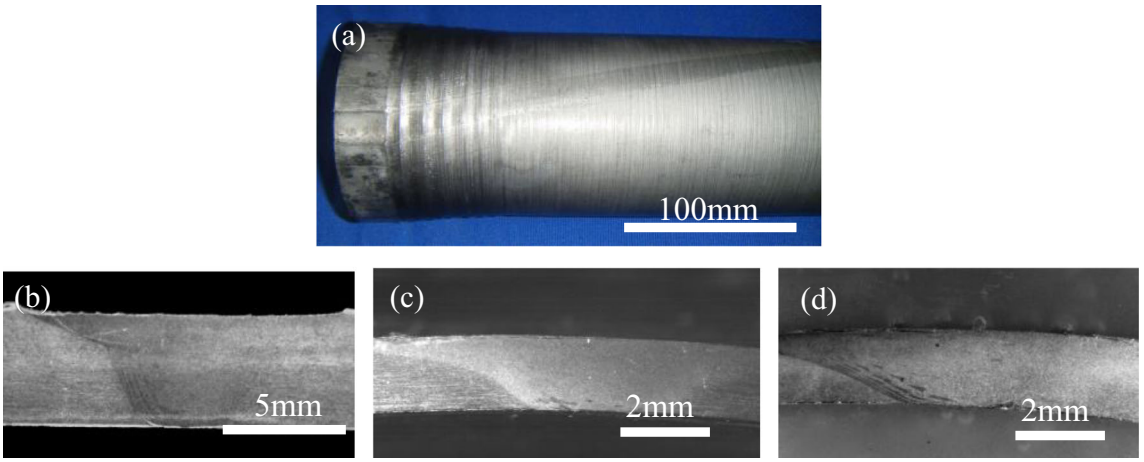

Fig. 3 Friction stir welded tube: **a** as-formed tube, **b** cross section of the as-welded joint, **c** cross-section of the as-spun joint, and **d** cross section of the heat treatment joint

Figure 4 presents the FSW tube after hydroforming. The tube bursts in the vicinity of the weld due to excessive thinning with a limit bugling rate of 15.1 % (Fig. 4a). Therefore, a two-step forming approach is adopted. First, a ring with a diameter of 124 mm and a thickness of 5 mm is put into the die, which is aiming to decrease the first expansion of the tube. A preformed part with a bugling rate of 10 % is obtained as shown in Fig. 4b. Then, the ring is removed and the final part with a bugling rate of 20 % is obtained as shown in Fig. 4c. No cracking or bursting is observed.

3.2 Thinning distribution of FSW tube with a spiral weld

Figure 5 shows the thinning distribution of tubes along the axial direction. It is found that thinning distribution of FSW tube along axial direction exhibits an M shape. Severe thinning is observed at one quarter of the expansion zone from symmetry plane. The thinning rate is about 19 %. For the two ends and symmetry plane of tube, the thinning is relatively small, which is about 13 %. This uneven thinning distribution of tube is more obvious along 0° direction, which passes through the weld. It is mainly because that the strength and the stress state for the weld and BM are different, caused by the spiral weld, which will be discussed in Sect. 4.3.

Figure 6 shows the thinning distribution at middle cross section of the tubes along the circumferential direction. The great thinning in the vicinity of the weld and the area opposite the weld zone (nearly 180°) is observed for the tube with variable diameter and the free bulging tube. Although the bulging rate of the tube is larger than that of the free bulging tube (Fig. 4a), it shows a relatively uniform thinning distribution compared to that of the free bulging tube (Fig. 6). The thinning rate of weld is about 13 %, and the average thinning rate of the BM is about 15 %. The difference of the thinning rate between weld and the BM is little. From a preform point of view, it is mainly because that the most vulnerable thinning location of the tube will contact with the die at early stage during hydroforming. The location of the tube no longer deforms or deforms little due to the large friction between the tube and die. Thus, the plastic deformation will be transferred to surrounding material which results in the relatively uniform deformation. In this way, the final tube shows the homogeneous thickness distribution. It is indicated that increases in the times of contacting die for FSW tube are able to improve the deformation uniformity of the tube and avoid excessive local thinning.

Fig. 4 The part formed by hydroforming: **a** typical fracture appearance of the FSW tubes, **b** the preformed part with a expansion ratio of 10 %, and **c** the finish part with a expansion ratio of 20 %

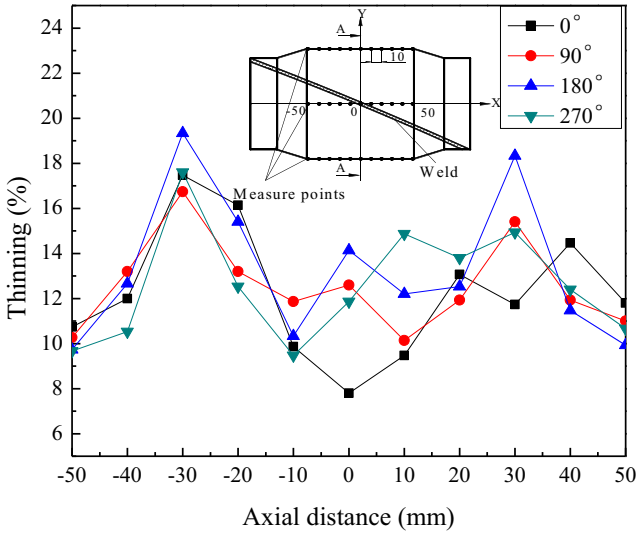

Fig. 5 Axial thinning distributions of the spiral weld tube in the expansion zone

4 Finite element analysis

4.1 Analysis model

An explicit finite element code LS-DYNA is adopted to analyze the plastic deformation of the welded tube during hydroforming for better understanding the thinning distribution characteristic of tubes experimentally observed. One of the most important factors to be considered when performing a numerical analysis is to use a constitutive model that accurately captures the behavior of the material. Kuwabara had done lots of work on the anisotropic plastic deformation behavior of tubular materials used for hydroforming automotive parts [22, 23]. By comparing the experimental observations with numerical predictions, it is concluded that the Yld2000 yield function is an effective phenomenological plasticity model for predicting the anisotropic plastic deformation behavior of the material [23]. However, the yield criteria needs at least seven parameters to describe both the uniaxial and the biaxial behavior, which barricades the wide use of the industry. Jansson et al. reported that Barlat-Lian's yield function was able to describe the behavior of orthotropic sheet metals under a general plane stress state, and was widely used in hydroforming simulations because of its mathematical simplicity compared with Yld2000 [24]. Barlat and Lian presented the anisotropic yield criterion for plane stress as follows:

$$f = a|K_1 + K_2|^m + a|K_1 - K_2|^m + c|2K_2|^m - 2\sigma_f^m\left(\frac{p}{\varepsilon}\right) = 0 \quad (1)$$

$$K_1 = \frac{\sigma_{11} + h\sigma_{22}}{2} \quad (2)$$

$$K_2 = \sqrt{\left(\frac{\sigma_{11} - h\sigma_{22}}{2}\right)^2 + (p\sigma_{12})^2} \quad (3)$$

Similar to Hill's yield criterion, four anisotropy parameters need to be determined, namely a, c, h, and p. The parameter m can be seen as a material parameter of its own. It is suggested to be equal to 8 for FCC metals [25].

In this work, the tube is meshed by Barlat's three-parameter plasticity model, and the dies are meshed by rigid elements. The type of element used to simulate the FSW tube is four-node shell element. The FE model is shown in Fig. 7. The FE mesh size for the tube and die is 3 and 5 mm, respectively. The total number of elements used to simulate the FSW tube and die is 14,324 and 8,114. The weld zone properties as well as geometry are included and the corresponding constitutive models of the weld and BM are considered as

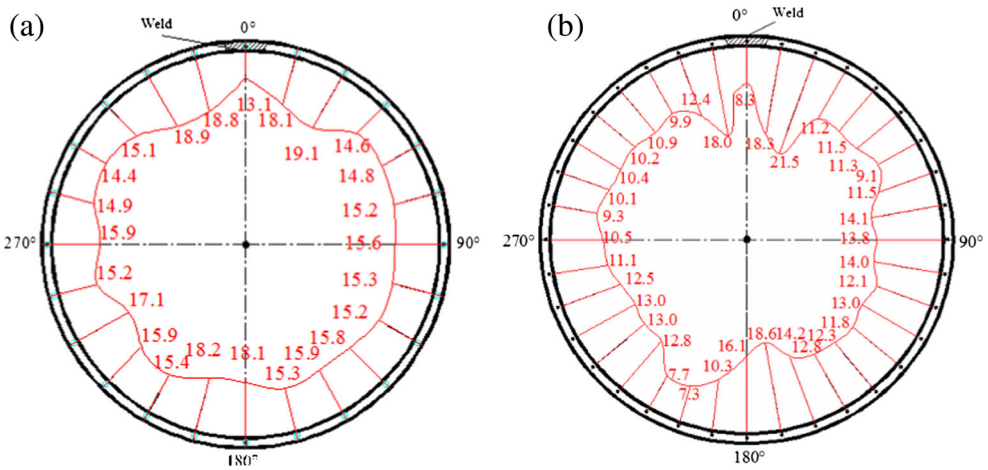

Fig. 6 Thinning at middle cross section of the tubes along the circumferential direction (%): **a** the tube with variable diameter and **b** the free bulging tube

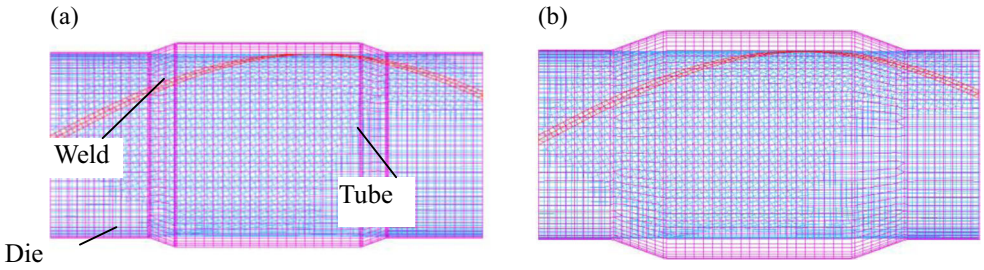

Fig. 7 FE mesh for the tube hydroforming process with variable diameter: **a** preform model and **b** hydroforming model

shown in Table 1. The tube material obeys the power hardening law represented by $\sigma=k\varepsilon^{n}$. The weld zone is 6 mm wide according to the measurements made with the cross-sectional macrographs of FSW joint. The microstructure of the weld zone is mainly composed of fine equiaxed grain according to the study of the Hu [19], which shows isotropy. Therefore, its mechanical property would be homogeneous. It is assumed that the weld material is isotropic and obeys Mises yielding criterion. Coulomb friction model is used and the friction coefficient assigned is 0.1. It is known that tensile test data for base material given as input to finite element model contains limited data of up to finite strain levels. In process simulations via finite element method (FEM), the tensile test stress–strain (σ–ε) curve is always extrapolated in the large strain range from power law.

For the tube with forced end condition during hydroforming, Lang et al. concludes that there are mainly two types of loading path: the linear variation method and the bilinear variation method. The bilinear variation method is reported to be more effective [26]. In the method, two stages can be distinguished, namely the preform stage and the calibration stage, respectively. First, the internal pressure is kept as a constant during axial feeding to form the useful wrinkles and then is increased as much as possible to flatten the wrinkles. But, if the wrinkles cannot be flattened in the calibration stage, the forming process is a failure and the wrinkles are called dead wrinkles. Figure 8 is the loading paths used in the simulation.

Table 1 Mechanical property of weld and BM

Parameters	Weld	BM
Young's modulus, E (MPa)	98,000	69,000
Poisson ratio, ν	0.33	0.33
Yield strength, σ_s (MPa)	193	175
Tensile strength, σ_t (MPa)	233	217
Hardening coefficient, *K* (MPa)	403	331
Strain hardening, *n*	0.2	0.17
Anisotropy coefficient, R_0	1	0.66
Anisotropy coefficient, R_{45}	1	0.79
Anisotropy coefficient, R_{90}	1	0.6

BM base material

4.2 Thickness distribution of the tube

Figure 9 shows the thickness distribution of the tube with a spiral weld. Generally speaking, the thickness of the weld is larger than that of the BM along the spiral weld (Fig. 9a). As for the thickness distribution of three typical cross sections of the tube, the thicknesses of the weld and the BM at middle cross section (B-B section) are larger than that at the each ends of the tube (A-A and C-C section), which is in agreement with the experiment result. In the hoop direction, the cross sections of the tube show the same thickness distribution characteristic. The weld shows the largest thickness, but the severe thinning in the vicinity of the weld is observed. In the cross section, the thicknesses of the points 1 and 5 are smaller than those of the other points, as shown in Fig. 9. Especially, for the point 5, its thickness is the minimum among the points for all the cross sections.

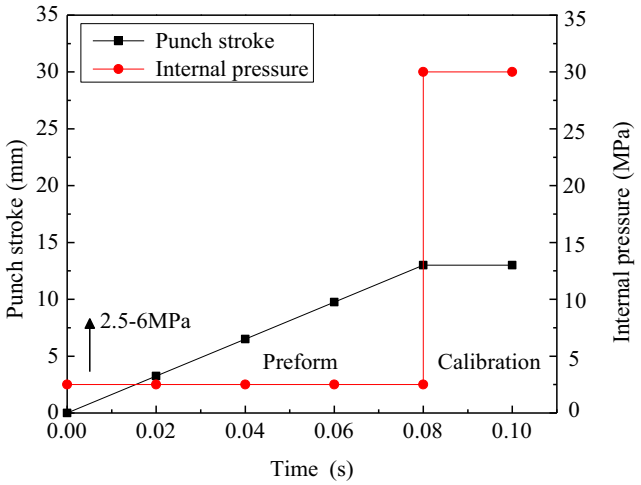

Fig. 8 Bilinear loading path used in the simulation

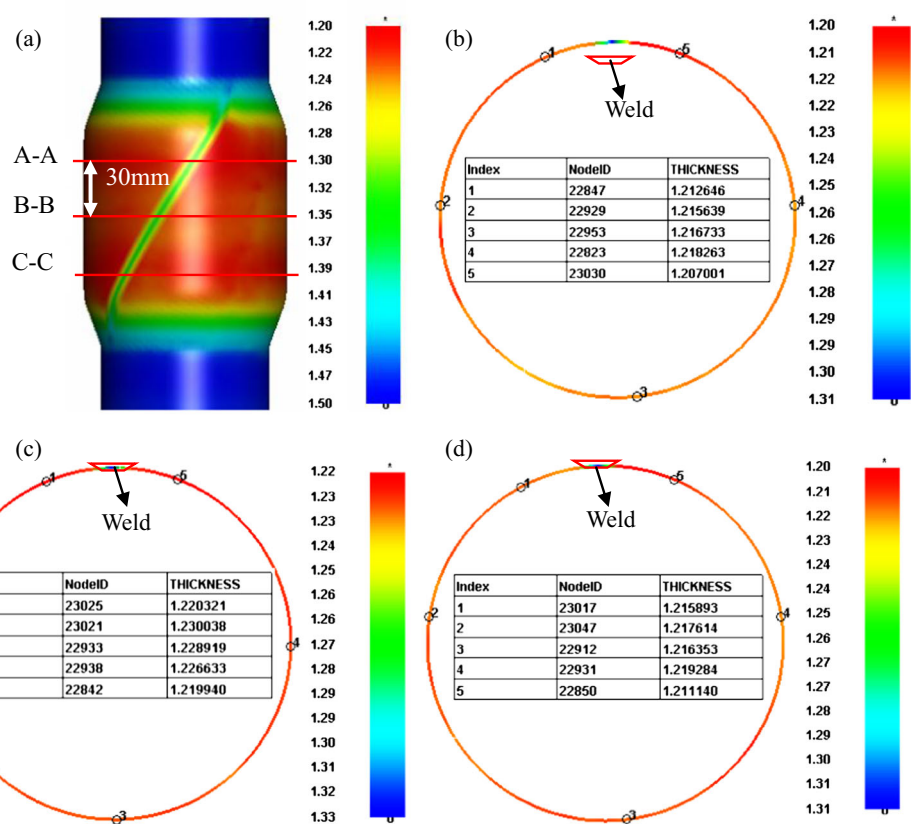

Fig. 9 Thickness distribution of welded tube: **a** global thickness distribution, **b** thickness distribution at A-A section, **c** thickness distribution at B-B section, and **d** thickness distribution at C-C section

4.3 Plastic deformation characteristics of FSW tube with a spiral weld

4.3.1 Plastic deformation of the typical cross section without axial feeding

Thickness distribution characteristics of the tube with a spiral weld can be well explained by the plastic deformation of the typical cross section. Figure 10 shows the curvature radius and stress state of feature points at the ends of the tube (A-A section). It can be seen that the curvature radius of the weld (feature point W_0) is the maximum. It is mainly because that the strength of the weld is slight higher than that of the BM; thus, the deformation of the weld is smaller compared to that of the BM, and the distance between the weld and the die

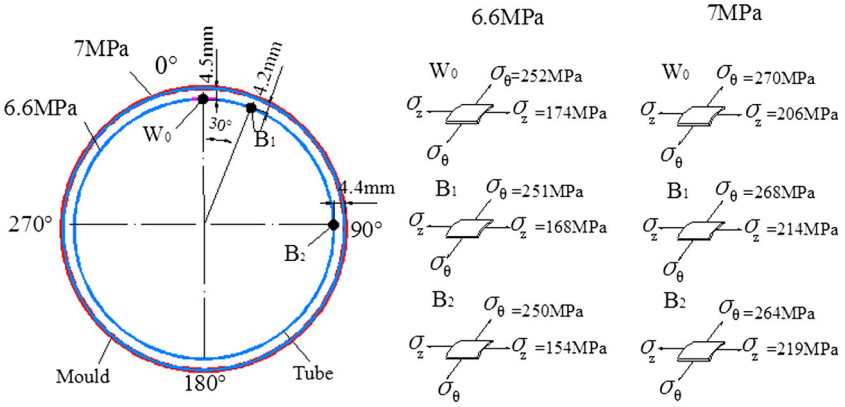

Fig. 10 The curvature radius and stress states at the end of the tube (A-A section)

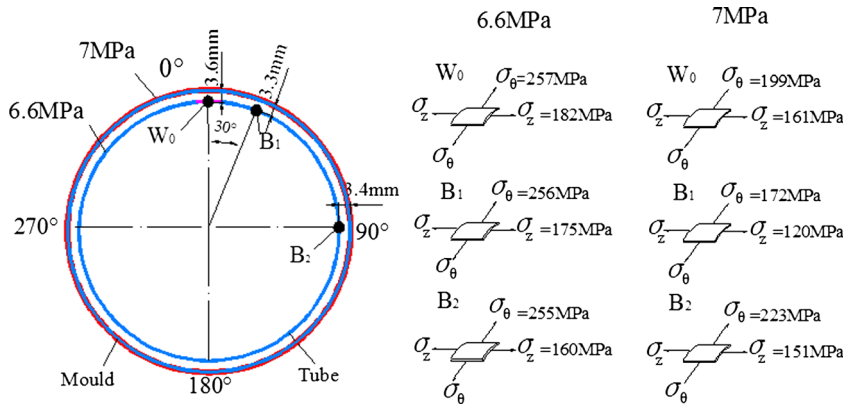

Fig. 11 The curvature radius and stress states at middle cross section of the tube (B-B section)

is the largest. By taking equilibrium of forces for the thin-walled tube under internal pressure, the following equations are derived:

$$\sigma_\theta = \frac{Pr^2}{d_0 t_0} \tag{4}$$

$$\sigma_z = \frac{2Pr^2}{d_0 t_0} \tag{5}$$

where P is the internal pressure, t_0 is the original wall thickness of the tube, d_0 is the initial outer radius of the tube, and r is the curvature radius of the tube.

From the Eqs. (4) and (5), it is found that the axial and circumferential stress depends on the curvature radius of the deformed tube under certain internal pressure. Thus, the hoop and axial stress of the weld (W_0) is higher than that of the BM as shown in Fig. 10. However, the strength of the weld is also higher. The deformation of the weld is small and the thickness is higher than that of the BM. Moreover, it is seen that the curvature radius of the BM close to the weld (feature point B_1) is larger than that of the others BM (feature point B_2) due to the deformation coordination between the weld and the BM. Therefore, the hoop and axial stress of the feature point B_1 is also higher than that of the feature point B_2, consequently resulting in severe thinning at point B_1 compared to the other BM.

Figure 11 shows the curvature radius and stress state of feature points at middle cross section of the tube (B-B section). The variation of curvature radius for the feature points is the same with that of the A-A section. But, the stress of the feature points in the B-B section is higher than that in the A-A section. As the pressure increases from 6.6 to 7 MPa, the circumferential and axial stress of the feature points in the B-B section decreases. However, the stress of the feature points in the A-A section increases with increasing pressure. It is known that the stress of the point will decrease when the point contacts the die. Thus, it is expected that the B-B section contacts the die earlier than the A-A section.

The thickness distribution during hydroforming greatly depends on the sequence of the contacting die of the tube. Figure 12 illustrates the contacting die process of the typical section of the tube. In the axial direction, the distance between the B-B section and die is small as the pressure is 6.6 MPa, but at this time, the A-A section is still far from the die as shown in Fig. 12a. When the pressure is 7 MPa, the contacting die of the B-B section is completed. But, the A-A section just starts the contacting die process. The deformation of the B-B section is little after finishing the contacting die due to the large friction between the die and tube. Simultaneously, the A-A section

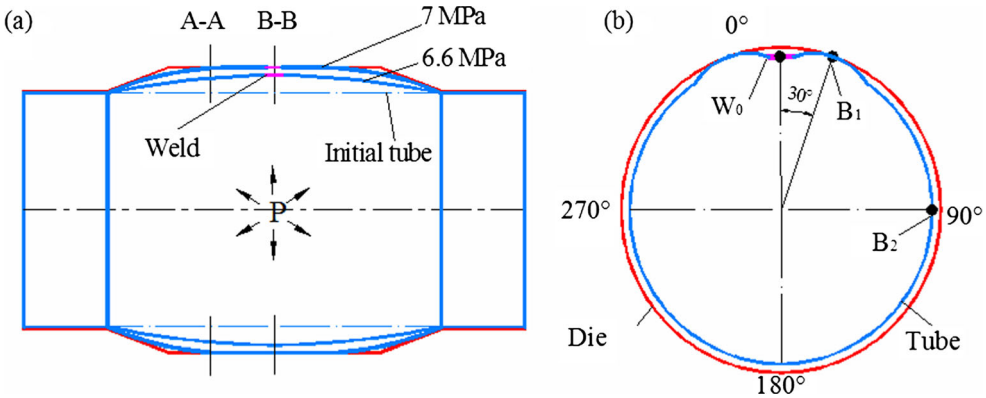

Fig. 12 Variations of the cross section of the FSW tube during hydroforming: **a** contacting die process of tube along axial direction and **b** contacting die in hoop direction

Table 2 Simulated results of the tubes under bilinear loading path

Pressure (MPa)	Thinning (%)	Number of wrinkles	Forming results
2.5	–	2	Dead wrinkles
3.0	11.9	3	Good
3.5	10.0	3	Good
4.0	11.2	3	Good
4.5	9.4	3	Good
5.0	11.5	3	Good
5.5	–	2	Dead wrinkles
6.0	–	–	Burst

continues to deform with increasing pressure, leading to the severe thinning in the A-A section compared to B-B section as observed in the experiment. In the hoop direction, it is seen that the feature point B_1 shows the minimum distance from the die as the pressure is 6.6 MPa. Simultaneously, the feature point B_1 suffers the largest stress among the other BM. Therefore, it is expected that the BM near the weld in the cross section contacts die first as shown in Fig. 12b, and would play a pinning effect for the deformation of weld. Thus, the thinning of the weld is relatively small.

4.3.2 Wrinkling behavior in hydroforming with axial feeding

The simulated results of the tubes under bilinear loading path during hydroforming are shown in Table 2. It is found that the part can be formed successfully when the internal pressure is 3.0–5.0 MPa. Especially, as the pressure is 3.5 or 4.5 MPa, the thinning rate of the part is only 10 and 9.4 %. The dead wrinkles can be observed during hydroforming when the pressure is 2.5 and 5.5 MPa. Moreover, bursting occurs at the wrinkle wave during calibration when the pressure is 6 MPa. It is noted that the material model does not include a failure criteria to predict the necking initiation after the uniform deformation part. Here a failure criteria is used based on a strain limit in the experimental results. It is considered a failure when the plastic strain has reached 15 %.

To investigate the effect of the weld on wrinkle behavior of the tube in detail, the comparison of plastic deformation for the welded tube and seamless tube during hydroforming is examined, as shown in Fig. 13. When the pressure is 2.5 MPa, two wrinkles occur at each ends of the welded tube. However, three wrinkles can be found for the seamless tube. As the pressure increases to 3 MPa, three wrinkles also occur in the welded tube. By comparison with the seamless tube, it is found that the radius of the wrinkle for the seamless tube is larger than that for the welded tube. It is known that the larger the radius of the wrinkle, the easier the wrinkle can be flattened in the calibration stage. It is indicated that the weld shows an inhibition for generation of the wrinkles or decrease of the number of the wrinkle during hydroforming. This effect is obvious when the pressure is low. However, as the pressure increases, the difference of the wrinkle behavior between the welded tube and seamless tube is small, as shown in Fig. 13. Moreover, it is noted that the distance between the two wrinkles is too near when the pressure is low. However, the distance and shape of the wrinkles are improved as pressure increases, and the distribution of the wrinkles is also more uniform.

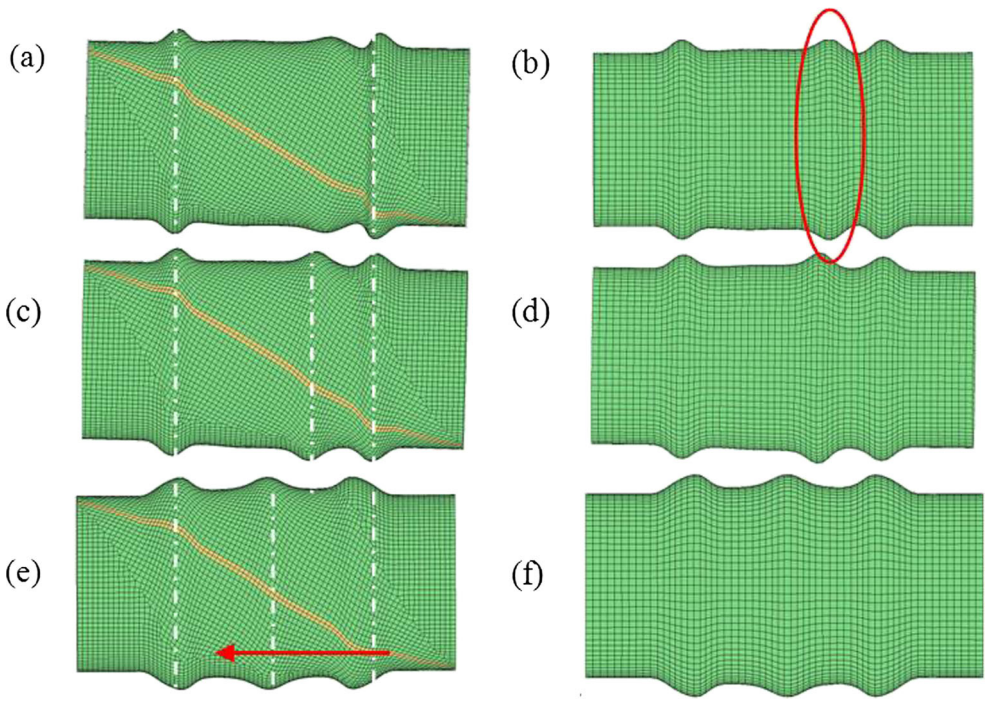

Fig. 13 Comparison of the wrinkle behavior for the welded tube and seamless tube during hydroforming: **a** 2.5 MPa for welded tube, **b** 2.5 MPa for seamless tube, **c** 3 MPa for welded tube, **d** 3 MPa for seamless tube, **e** 4.5 MPa for welded tube, and **f** 4.5 MPa for seamless tube

Fig. 14 Wrinkle behavior for the welded tube during hydroforming: **a** 2.5 MP, **b** 3 MPa, and **c** 4.5 MPa

Figure 14 shows the experimental result of the wrinkle behavior for the welded tube during hydroforming. It can be seen that two wrinkles occur at each ends of the welded tube as internal pressure is 2.5 MPa, which is as same as the simulation. However, the radius of the wrinkle is too small (Fig. 14a). It is mainly because that the internal pressure is too low compared with the punch stroke, and folding back failure should be induced. When the internal pressure is 3 MPa, the number of the wrinkles in the expansion zone increases and three wrinkles can be observed. Moreover, the shape of the wrinkles is also improved. It indicates that the simulated results can direct the experiment very well. But, the distance between the two wrinkles is too near. As the internal pressure increases to 4.5 MPa, although the number of the wrinkles no longer increases, the distribution and shape of the wrinkles are improved. It can be expected that these useful wrinkles can be flattened in the calibration stage. It is indicated that the radius of the wrinkle increases with increasing the internal pressure, and the distance between wrinkles also increases.

5 Conclusions

2024 Al alloy FSW tubes were produced using a novel processing technique. The hydroforming characteristics of FSW tube with a spiral weld were experimentally and numerically investigated. The following conclusions are drawn from the results of this study:

1. Thickness distribution law of the tube with a spiral weld is obtained based on experimental result. It is found that the thinning of the tube in axial direction shows an M-shaped distribution. Severe thinning is observed at one quarter of the expansion zone from symmetry plane, but the thinning in the ends of tube including symmetry plane is small. In the hoop direction, the BM around the weld experiences severe thinning with a thinning rate of 19 %, while the average thinning rate of the other BM is about 15 %. Compared with thinning rate of the tube in the free bulging, it is indicated that the uniformity of thickness distribution can be improved by pre-forming.
2. The relationship among the thickness distribution, cross-sectional shape, and stress state of spiral weld tube during hydroforming is revealed by numerical simulations. It is found that cross section of the FSW tube is no longer circular due to the presence of the weld. The radius of the base metal adjacent weld is greater than that of other BM and thus suffers higher hoop and axial tensile stress, which lead to severe thinning.
3. The contacting die process of the typical section for the FSW tube is illustrated. In the axial direction, the contacting die process of the symmetry plane is completed, while the plane at each end of the tube is still far from the die. The circumferential and axial stress of the plane at each end increases with increasing pressure and consequently leads to severe thinning. In the hoop direction, the BM near the weld in the symmetry plane contacts die first due to the high circumferential and axial stress, which plays a pinning effect for the deformation of weld. Thus, the thinning of the weld is relatively small.
4. The weld shows an inhibitory effect for generation of the wrinkles and decreases the number of the wrinkles during hydroforming as compared to the seamless tube. This effect is more obvious when the forming pressure is lower. However, as the forming pressure increases, the difference of the wrinkle behavior between the welded tube and seamless tube decreases.
5. The good mechanical properties of the weld proved that the use of friction stir welded tubes, for example in hydroforming, can be a valid solution for some industrial applications. Also, it is confirmed that the FSW weld shows significant effect on the thickness of the tube during hydroforming. Careful attention must be given to the processing route of hydroforming FSW tube to ensure the uniformity of the thickness.

Acknowledgments This study is financially supported by National Natural Science Foundation of China (Grant No. 51405358), the China Postdoctoral Science Foundation funded project (2014M560632), Fundamental Research Funds for the Central Universities (WUT: 2014-IV-042), and State Key Laboratory of Materials Processing and Die & Mould Technology (P 2015- 05), Huazhong University of Science and Technology. The authors would like to take this opportunity to express their sincere appreciation.

References

1. Dohmann F, Hartl C (1996) Hydroforming—a method to manufacture light-weight parts. J Mater Process Technol 60:669–676
2. Chu GN, Liu G, Liu WJ, Yuan SJ (2012) An approach to improve thickness uniformity. Int J Adv Manuf Technol 60:1247–1253
3. Alaswad A, Benyounis KY, Olabi AG (2012) Tube hydroforming process: a reference guide. Mater Des 33:328–339
4. Buffa G, Fratini L, Hua J, Shivpuri R (2006) Friction stir welding of tailored blanks: investigation on process feasibility. CIRP Ann 55: 279–282
5. Sato YS, Sugiura Y, Shoji Y, Park SHC, Kokawa H, Ikeda K (2004) Post-weld formability of friction stir welded Al alloy 5052. Mater Sci Eng A 369:138–143
6. Miles MP, Decker BJ, Nelson TW (2004) Formability and strength of friction-stir-welded aluminum sheets. Metall Mater Trans A 35A: 3461–3468
7. Fratini L, Piacentini M (2006) Friction stir welding of 3d industrial parts: joint strength analysis. In: ASME proceedings of the 8th biennial conference on engineering systems design and analysis. Turino, pp 763-770
8. Dubourg L, Gholipour J, Jahazi M (2008) Friction stir welding of 2024-T3 aluminum tubes for hydroforming application. In: Trends in welding research, proceedings of the 8th international conference. Pine Mountain, GA, pp 549–556
9. Marré M, Ruhstorfer M, Tekkaya AE, Zaeh MF (2009) Manufacturing of lightweight frame structures by innovative joining by forming processes. Int J Mater Form 2:307–310
10. Urso GD, Longo M, Giardini C (2013) Mechanical and metallurgical analyses of longitudinally friction stir welded tubes: the effect of process parameters. Int J Mater Prod Technol 46:177–196
11. Urso GD, Longo M, Giardini C (2011) Characterization of friction stir welded tubes by means of tube bulge test. The 14th international esaform conference on material forming: ESAFORM 1353: 1259–1264.
12. Leitao C, Leal RM, Rodrigues DM, Loureiro A, Vilaca P (2009) Tensile behavior of similar and dissimilar AA5182-H111 and AA6016-T4 thin friction stir welds. Mater Des 30:101–108
13. Aval HJ, Serajzadeh S (2014) A study on natural aging behavior and mechanical properties of friction stir-welded AA6061-T6 plates. Int J Adv Manuf Technol 71:933–941
14. Ipekoglu G, Erim S, Cam G (2014) Effects of temper condition and post weld heat treatment on the microstructure and mechanical properties of friction stir butt-welded AA7075 Al alloy plates. Int J Adv Manuf Technol 70:201–213
15. Silva MB, Skjoedt M, Vilaca P, Bay N, Martins PAF (2009) Single point incremental forming of tailored blanks produced by friction stir welding. J Mater Process Technol 209:811–820
16. Kim DY, Lee W, Kim JY, Chung KH, Kim CM, Okamoto K, Wagoner RH, Chung K (2010) Macro-performance evaluation of friction stir welded automotive tailor-welded blank sheets: part II – formability. Int J Solids Struct 47:1063–1081
17. Ramulu PJ, Ganesh NR, Kailas SV (2013) Forming limit investigation of friction stir welded sheets: influence of shoulder diameter and plunge depth. Int J Adv Manuf Technol 69: 2757–2772
18. Hu ZL, Yuan SJ, Wang XS, Liu G, Huang YX (2011) Effect of post-weld heat treatment on the microstructure and plastic deformation behavior of friction stir welded 2024. Mater Des 32:5055–5060
19. Hu ZL, Yuan SJ, Wang XS, Liu G, Liu HJ (2012) Microstructure and mechanical properties of Al–Cu–Mg alloy tube fabricated by friction stir welding and tube spinning. Scr Mater 55:637–640
20. Yuan SJ, Hu ZL, Wang XS (2012) Evaluation of formability and material characteristics of aluminum alloy friction stir welded tube produced by a novel process. Mater Sci Eng A 543:210–216
21. Fatemi A, Morovvati MR, Biglari FR (2013) The effect of tube material, microstructure, and heat treatment on process responses of tube hydroforming without axial force. Int J Adv Manuf Technol 68: 263–276
22. Kuwabara T (2007) Advances in experiments on metal sheets and tubes in support of constitutive modeling and forming simulations. Int J Plast 23:385–419
23. Kuwabara T, Yoshida K, Narihara K (2005) Anisotropic plastic deformation of extruded aluminum alloy tube under axial forces and internal pressure. Int J Plast 21:101–117
24. Jansson M, Nilsson L, Simonsson K (2005) On constitutive modeling of aluminum alloys for tube hydroforming applications. Int J Plast 21: 1041–1058
25. Barlat F, Lian J (1989) Plasticity behavior and stretchability of sheet metals Part 1: a yield function for orthotropic sheets under plane stress conditions. Int J Plast 5:51–66
26. Lang LH, Yuan SJ, Wang ZR, Wang XS, Danckert J, Nielsen KB (2004) Experimental and numerical investigation into useful wrinkling during aluminum alloy internal high-pressure forming. Proc IME B J Eng Manufact 218:43–49